Noname manuscript No.
(will be inserted by the editor)

Coupled dynamics for superfluid ^{4}He in the channel.

D. Khomenko · P. Mishra · A. Pomyalov

arXiv:1608.06162v1 [cond-mat.other] 22 Aug 2016

Received: date / Accepted: date

Abstract We study the coupled dynamics of normal and superfluid components of the superfluid ^{4}He in the channel considering the counterflow turbulence with laminar normal component. In particular, we calculated profiles of the normal velocity, the mutual friction, the vortex line density and other flow properties and compared them to the case when the dynamic of the normal component is "frozen". We have found that the coupling between the normal and superfluid components leads to flattening of the normal velocity profile, increasingly more pronounced with temperature, as the mutual friction, and therefore coupling, becomes stronger. The commonly measured flow properties also change when the coupling between two components is taken into account.

Keywords Superfluid helium · Coupled Dynamics · Thermal Counterflow

1 Introduction

Superfluid ^{4}He below transition temperature $T_\lambda \simeq 2.17\,\mathrm{K}$ may be viewed as a two-fluid system[1,2,3] consisting of normal fluid with the very low kinematic viscosity $\nu_\mathrm{n}(T)$ and inviscid superfluid component, that have their own densities, $\rho_\mathrm{n}(T)$, $\rho_\mathrm{s}(T)$, and velocity fields, $\boldsymbol{u}_\mathrm{n}(\boldsymbol{r},t)$, $\boldsymbol{u}_\mathrm{s}(\boldsymbol{r},t)$. Due to quantum mechanical restriction, the circulation around the superfluid vortices is equal to $\kappa = h/m \simeq 10^{-3}\,\mathrm{cm}^2/\mathrm{s}$, where h is the Plank constant and m denotes the mass of ^{4}He atom. The singly quantized vortices usually arrange themselves in a tangle, referred to as *quantum turbulence*, that may be characterized by vortex line density (VLD) $\mathcal{L}$, i.e., total length of the quantized vortex line in a unit volume.

The large scale motion of such a system may be described by Hall-Vinen-Bekarevich-Khalatnikov equations(HVBK)[6,7], where both components are

D. Khomenko · P. Mishra · A. Pomyalov
Department of Chemical Physics, Weizmann Institute of Science, 76100 Rehovot, Israel
E-mail: dmytro.khomenko@weizmann.ac.il

considered as continuous fluids, coupled by a mutual friction force. The microscopic description of the vortex lines dynamics at scales that are still much larger than the vortex core size $a_0 \approx 10^{-8}$ cm, was proposed by Schwarz[13, 14] in the framework of Vortex Filament Method (VFM). In his approach, the influence of the normal component the dynamics on the quantum vortex lines is accounted through the mutual friction force with the predefined time-independent normal fluid velocity. It was soon realized that the back-reaction of the vortex tangle on the dynamics of the normal component may be important and several self-consistent methods, coupling Navier-Stokes equation for the normal component with Lagrangian description of the vortex lines dynamics, were proposed[8,9,10]. These methods are computationally challenging, given the wide range of scales involved in the problem. Such a self-consistent studies were limited to space-homogeneous flows with diluted vortex tangles.

The VFM methods were extended to the wall-bounded flows[15,16] and more recently included full Biot-Savart description of the tangle [17,18,19, 20]. Also here, a time-independent mean normal velocity profile, or a snapshot of the turbulent velocity field were imposed to generate the quantum vortex tangle.

Depending on the way the quantum turbulence is generated in the channel or pipe, the normal and superfluid components flow in the same direction, or in opposite directions. In the latter case (the thermal counterflow), a relative, counterflow velocity $V_{\rm ns}$ is established in the channel. At sufficiently large values of $V_{\rm ns}$ the quantum vortex tangle is created. As $V_{\rm ns}$ increases, the thermal counterflow passes several stages. At relatively low values of counterflow velocity, the normal components remains laminar, while a fully-developed quantum vortex tangle is formed, indicating superfluid turbulence. This regime was labeled at T1 state [21]. At higher values of $V_{\rm ns}$, the normal component also becomes turbulent, forming so-called T2 state.

In this paper we address the back-reaction of the quantum vortex tangle on the normal velocity profile, restricting our study to T1 state of the counterflow in the channel. Here we describe the laminar normal velocity by its mean profile (neglecting normal velocity fluctuations), but allow its evolution, driven by the mutual friction force that couples dynamics of the mean normal velocity with the evolution of the vortex tangle. To be consistent with the nature of the mean profile, the mutual friction force, generated by the vortex tangle, is integrated over space and short intervals of time. Such a multi-scale, multi-time approach allows us to follow the coupled dynamics of two components and account for the influence of the vortex tangle on the normal component.

We have found that initially parabolic mean normal velocity profile evolves to a flatter shape, with effect stronger for higher temperature and counterflow velocities. As a consequence, the VLD profile becomes more uniform in the channel core with the peaks pushed towards the wall. Both the global and microscopic properties of the flow change compared to the uncoupled dynamics, although this effect is significant only at high temperatures.

2 Coupled system

In the framework of two-fluid description of the superfluid ^{4}He, dynamics of the normal component is given by HVBK equation[6,7,8]:

$$\frac{\partial \boldsymbol{u}_{\rm n}}{\partial t} + (\boldsymbol{u}_{\rm n}\cdot\nabla)\boldsymbol{u}_{\rm n} = \frac{\nabla P}{\rho_{\rm n}} + \frac{\boldsymbol{F}_{\rm ns}}{\rho_{\rm n}} + \nu_{\rm n}\Delta\boldsymbol{u}_{\rm n}, \tag{1}$$

where mutual friction force $\boldsymbol{F}_{\rm ns}$ couples the two components and the effective pressure P is defined by: $\nabla P = -\rho_{\rm n}/\rho\ \nabla p + \rho_{\rm s} S\nabla T$ (S is entropy and $\rho = \rho_{\rm n} + \rho_{\rm s}$ is density of Helium II). For the laminar flow in the channel, Eq. (1) simplifies to an equation for the mean normal velocity:

$$\frac{\partial V_{\rm n}(y)}{\partial t} = \frac{dP}{dx} + \frac{\mathcal{F}_{\rm ns}(y)}{\rho_{\rm n}} + \nu_{\rm n}\frac{\partial^2 V_n(y)}{\partial y^2}, \tag{2}$$

Here we took into account that in the planar channel geometry the normal velocity field $V_{\rm n}(y)$ depends on the wall-normal direction only and has only one non-zero (streamwise) component along channel. The mutual friction term $\mathcal{F}_{\rm ns}(y)$ is a time average of a streamwise projection of the mutual friction force,

$$\boldsymbol{F}_{\rm ns} = \frac{\rho_s}{\Omega}\int_{\mathcal{C}'}(\alpha\boldsymbol{s}'\times[\boldsymbol{s}'\times\boldsymbol{V}_{\rm ns}] + \alpha'\boldsymbol{s}'\times\boldsymbol{V}_{\rm ns})d\xi, \tag{3}$$

defined by dynamics of the quantum vortex tangle[14]. Here $\boldsymbol{s}$ is a radius vector to the points on the vortex line, $'$ denotes derivative along the vortex line and α, α' are the mutual friction coefficients. The integral in Eq. (3) is taken along vortex lines $\mathcal{C}'$, residing inside suitably defined coarse-grained volume Ω.

The instantaneous counterflow velocity $\boldsymbol{V}_{\rm ns} = \boldsymbol{V}_{\rm n} - \boldsymbol{V}_{\rm s}$ is defined by velocities of the normal and superfluid components. The superfluid velocity $\boldsymbol{V}_{\rm s} = V_{\rm s}^0 + \boldsymbol{V}_{\rm BS}(\boldsymbol{s})$ contains contributions of the vortex tangle velocity $\boldsymbol{V}_{\rm BS}(\boldsymbol{s})$ in the Biot-Savart representation, integrated over entire vortex configuration $\mathcal{C}$ and the applied superfluid velocity $V_{\rm s}^0$, defined by the counterflow condition $\rho_{\rm n}\langle\boldsymbol{V}_{\rm n}\rangle_v + \rho_{\rm s}\langle\boldsymbol{V}_{\rm s}\rangle_v = 0$. Here $\langle ...\rangle_v$ stands for global volume averaging.

Implementation Details The simulations were set up in a planar channel of the size $4h\times 2h\times 2h, h = 0.05$ cm. The vortex-lines dynamics was solved using VFM[14,25,20] with 4th-order difference scheme for the derivatives $\boldsymbol{s}'$ and $\boldsymbol{s}''$ [23,24]. We used the periodic boundary condition in the streamwise(x) and the spanwise(z) directions, with slip conditions in the wall-normal y direction, the line-resolution $\Delta\xi_0 = 0.0016$ cm and the timestep $\delta t_{\rm s}$, defined by the

Table 1 Parameters of Heluim-II,used in simulations[26].

T(K)	α	α'	ρ_n (g/cm^3)	ρ_n/ρ_s	$\nu = \eta/\rho_n$ (cm^2/sec)
1.45	6.1×10^{-2}	1.8×10^{-2}	1.3×10^{-2}	1.0×10^{-1}	1.0×10^{-3}
1.6	9.7×10^{-2}	1.6×10^{-2}	2.4×10^{-2}	1.9×10^{-1}	5.6×10^{-4}
1.9	2.1×10^{-1}	8.3×10^{-2}	6.1×10^{-2}	7.2×10^{-1}	2.2×10^{-4}

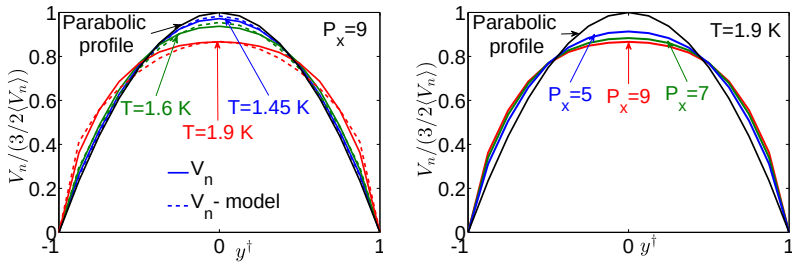

Fig. 1 Comparison of normalized velocity profiles $V_{\rm n}(y)/(3/2\ \langle V_{\rm n}\rangle)$ vs $y^\dagger = y/(h), y^\dagger \in [-1,1]$ for effective pressure gradient $P_{\rm x} = 9$ and different temperatures (left panel) and for $T = 1.9$K and different values $P_{\rm x}$ (right panel). The normalized parabolic profile is shown by black solid line. In the left panel we also show the model profiles Eq. (8)(dashed lines) for $T = 1.45$K[$\langle V_{\rm n}\rangle = 1.22$ cm/s], 1.6K[$\langle V_{\rm n}\rangle = 1.01$ cm/s]and 1.9K[$\langle V_{\rm n}\rangle = 0.69$cm/s]. Values of $A_{\rm GM}$, calculated from mutual friction force in the coupled dynamics are: $A_{\rm GM}(1.45) = 20.7$cm·s/g, $A_{\rm GM}(1.6) = 35.7$cm·s/g, $A_{\rm GM}(1.9) = 47.2$cm·s/g and $n = 14$.(Color Online)

stability condition of the 4th-order Runge-Kutta scheme. The dynamics of the mean normal velocity profile $V_{\rm n}(y,t)$, Eq. (2), was solved using 2nd-order finite-difference scheme for the viscous term, 2nd-order Adams-Bashforth method for the time marching and no-slip conditions on the solid walls. The effective pressure gradient $P_{\rm x} = dP/dx$ was used as a free parameter of the system.

To calculate the mutual friction term, we used two-stage approach. The term $\mathcal{F}_{\rm ns}$ in Eq. (2) implies averaging over space and time, while the term $F_{\rm ns}$ is instantaneous and is averaged only over space. The parabolic normal velocity profile was initiated on a grid of a mesh size $\delta y = 0.00625$ cm in the wall-normal direction. Using this profile, the superfluid system was propagated for $\Delta t = 10\delta t_{\rm s}$. At each time step, the mutual friction force $F_{\rm ns}$ was integrated over thin slices of volume $4h \times \delta y \times 2h$ and then averaged during Δt. Resulting values of $\mathcal{F}_{\rm ns}$ were assigned to the middle points of the slices in y-direction and linearly interpolated to the normal velocity grid points. With this mean mutual friction force, $V_{\rm n}(y)$ was then propagated to Δt using the same $\delta t_{\rm s}$. The newly obtained values of $V_{\rm n}(y)$ were interpolated to the positions of the

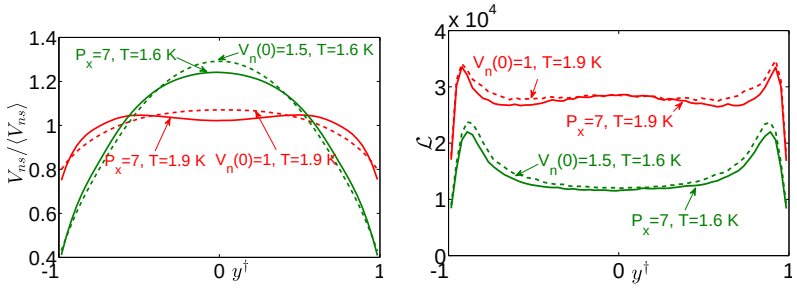

Fig. 2 Comparison of normalized $V_{\rm ns}$(left) and VLD profiles(right) for coupled dynamics (solid lines) and for time-independent parabolic $V_{\rm n}$ (dashed lines) for $T = 1.6$K and 1.9K.(Color Online)

line points for the next cycle of the superfluid dynamics, during which $V_{\rm n}$ was considered constant.

The resulting profiles of $\mathcal{L}(y)$, $V_{\rm s,n}(y)$ and other related properties were obtained by integrating over the same slices as the mutual friction, assigned to the middle points of the slices and then averaged over more than 50 steady-state configurations. The simulations were carried out for $T = 1.45, 1.6$ and 1.9 K and a number of $P_{\rm x}$ values. The material properties of the fluid components [26] are given in the Table 1. Notice that we didn't use the modified mutual friction coefficients[9], because we only consider the mean normal velocity field.

3 Results and Discussion

The steady-state profiles of $V_{\rm n}(y)$ for different T and values of effective pressure are shown in Fig. 1. To compare the shapes of profiles we normalized them by $3/2\ \langle V_{\rm n}\rangle$. For the original parabolic profile this value corresponds to the centerline velocity. For modified profiles this relation no longer valid. The profiles of $V_{\rm n}(y)$ become flatter in the center of the channel, increasingly so with increasing temperature and the applied pressure gradient. The resulting profile of counterflow velocity $V_{\rm ns}(y)$ is shown by solid lines in Fig. 2, left panel, for $T = 1.6$K and 1.9K together with profiles, obtained using time-independent parabolic profile with similar $\langle V_{\rm n}\rangle$(dashed lines). The flatter profiles of $V_{\rm n}$ lead to a change in the profiles of $V_{\rm ns}$, especially in the channel core. The vortex lines tend to concentrate in the regions with smaller $V_{\rm n}$[20], such that the peaks in the VLD profiles are pushed further toward the walls.

The statistical properties of the vortex tangle are commonly characterized by relation between mean VLD in the channel and $\langle V_{\rm ns}\rangle$: $\langle\mathcal{L}\rangle^{1/2} = \gamma(T)(\langle V_{ns}\rangle - v_0)$, where $\gamma(T)$ is a temperature-dependent coefficient and v_0 is virtual origin. This relation is valid only globally[27]. We compare in Table 2 the values of γ, obtained with different profiles. Notice that results for different profiles at temperatures $T = 1.45$K and 1.6K are close, while for higher $T = 1.9$K, $\gamma_{\rm c}$ is significantly larger than $\gamma_{\rm p}$. The values of $\gamma_{\rm p}$ are close to those of uniform $V_{\rm n}$ for all temperatures. Notably, our results are higher than those, obtained in Refs.[18,19] for the channel counterflow with parabolic and Hagen-Poiseuille profiles. This discrepancy may stem from the fact that in both [18,19] the counterflow condition did not include contribution from the vortex tangle, which is not negligible for dense tangles.

Model profile of V_n To rationalize the observed modifications of the normal velocity profile, we notice that in steady state the mutual friction force is almost constant across the channel, except for the near-wall region, where it quickly falls to zero. Therefore, qualitatively, the mutual friction redefines the effective pressure gradient in the middle of the channel $P_x + \langle\mathcal{F}_{\rm ns}\rangle/\rho_{\rm n}$, while near the wall it remains P_x. Such a change leads to flattening of the normal velocity profile (as compared to classic parabolic profile).

Table 2 The values of $\gamma(T)$ for different profiles: $\gamma_{\rm c}$ for coupled dynamics, $\gamma_{\rm p}$ for frozen parabolic profile. For comparison we give also values for the parabolic profile, Ref.[18], the Hagen-Poiseuille profile $\gamma_{\rm hp}$[19] and for the uniform normal velocity $\gamma_{\rm uni}$[25].

T(K)	$\gamma_{\rm c}$ (s/cm^2)	$\gamma_{\rm p}$(s/cm^2)	$\gamma_{\rm p}$(s/cm^2) [18]	$\gamma_{\rm hp}$(s/cm^2)[19]	$\gamma_{\rm uni}$(s/cm^2)[25]
1.3	-	-	67.9	31	72.1
1.45	83	85	–	–	–
1.6	114	113	83.6	47	115.7
1.9	165	144	105.7	103	148

To find new, flattened, $V_{\rm n}$ we first model the shape of mutual friction force profile by a function:

$$\mathcal{F}_{\rm ns} = -(1 - {y^\dagger}^n)\mathcal{F}_{\rm ns}(0)\,, \tag{4}$$

where n is an even integer and $\mathcal{F}_{\rm ns}(0)$ is the mutual friction force in the middle of the channel. To account for the sharp transition from almost a constant value in the middle of the channel to zero at the wall, large values of n are required. In this work we use $n = 14$. Substituting (4) into steady state equation (2) for V_n we get:

$$\frac{\nu}{h^2}\frac{d^2V_{\rm n}}{d{y^\dagger}^2} = -P_{\rm x} + \frac{\mathcal{F}_{\rm ns}(0)}{\rho_n}(1 - {y^\dagger}^n)\,. \tag{5}$$

This equation is easily solved, giving:

$$V_{\rm n}(y^\dagger) = A\left(1 - {y^\dagger}^2\right)\left[1 + \frac{2C}{(n+2)(n+1)}\frac{1 - {y^\dagger}^{n+2}}{1 - {y^\dagger}^2}\right]\,, \tag{6}$$
$$A = h^2 P_{\rm x,m}/(2\nu)\,, C = \mathcal{F}_{\rm ns}(0)/(\rho_n P_{\rm x,m})\,, P_{\rm x,m} = P_{\rm x} - \mathcal{F}_{\rm ns}(0)/\rho_n\,.$$

Notice, that when mutual force is not taken into account $\mathcal{F}_{\rm ns}(0) = 0$, the profile (6) reduces to the classical parabolic profile. To proceed, we notice that $\langle V_n\rangle = 2A/3 + 2AC/[(n+1)(n+3)]$ and $\langle\mathcal{F}_{\rm ns}\rangle = n\mathcal{F}_{\rm ns}(0)/(n+1)$. Using counterflow condition and Gorter-Mellink relation between mean mutual friction force and $\langle V_{\rm ns}\rangle$, we find

$$\langle\mathcal{F}_{\rm ns}\rangle = A_{\rm GM}\rho_{\rm s}\rho_{\rm n}(1 + \rho_{\rm n}/\rho_{\rm s})^3\langle V_{\rm n}\rangle^3 \equiv \frac{\rho_n\nu}{h^2}\frac{\langle V_n\rangle^3}{V_0^2}\,. \tag{7}$$

The characteristic velocity $V_0 = \left(A_{\rm GM}\rho_s h^2(1 + \rho_{\rm n}/\rho_{\rm s})^3/\nu\right)^{-1/2}$ corresponds to a balance between mutual friction and viscous terms and $A_{\rm GM}$ is the Gorter-Mellink constant. Combining all above we finally get:

$$V_{\rm n}(y^\dagger) = \frac{3}{2}\langle V_{\rm n}\rangle\left[V_1(1 - {y^\dagger}^2) + V_2\left(1 - {y^\dagger}^{n+2}\right)\right]\,, \tag{8}$$

where $V_1 = \left(1 - \frac{1}{n(n+3)}\left[\frac{\langle V_{\rm n}\rangle}{V_0}\right]^2\right)$ and $V_2 = \frac{2}{3(n+2)n}\left[\frac{\langle V_{\rm n}\rangle}{V_0}\right]^2$ are T-dependent expansion coefficients. The model profiles are compared with numerical results in Fig1, left panel.

4 Conclusions

We have studied back-reaction of the quantum vortex tangle on the mean laminar normal velocity profile in the channel counterflow. The initially parabolic V_n evolves to a flatter shape. The vortex tangle influences the mean normal velocity profile via mutual friction force. As a result, both the global properties of flow and the profiles of microscopic properties of the tangle, such as rms curvature, change compared to the uncoupled dynamics, with effect being stronger for high temperatures and counterflow velocities. At low and moderate temperatures the flow and tangle properties are close to those with the time-independent normal velocity profile. We propose a model of $V_{\rm n}(y)$, expressed via $\langle V_{\rm n}\rangle$, that accounts for the effect of mutual friction.

Acknowledgements We acknowledge useful and encouraging discussions with V.L'vov and I. Procaccia.

References

1. C. F. Barenghi, L. Skrbek and K. R. Sreenivasan, Proc. Natl. Acad. Sci. USA **111**, 4647 (2014).
2. W. F. Vinen and J. J. Niemela, J. Low Temp. Phys. **128**, 167 (2002).
3. L. Skrbek and K.R. Sreenivasan, Phys. Fluids **24**, 011301 (2012).
4. R. J. Donnelly, *Quantized Vortices in Hellium II*, (Cambridge Univ. Press, 1991).
5. *Quantized Vortex Dynamics and Superfluid Turbulence*, edited by C. F. Barenghi, R. J. Donnelly and W .F. Vinen, Lecture Notes in Physics **571**, (Springer-Verlag, Berlin, 2001).
6. H.E. Hall, W.F. Vinen, Proc. R. Soc. Lond. A Math Phys. Sci. **238**, 215 (1956).
7. I.L. Bekarevich, I.M. Khalatnikov, Sov. Phys. JETP **13**, 643 (1961).
8. C. Barenghi and David C. Samuels, Phys. Rev. B **60**, 1252), 1999.
9. O.C. Idowu, D. Kivotides, C.F. Barenghi and D. C. Samuels, J. Low Temp. Phys., 120 (2000) 269.
10. Kivotides D., Barenghi C. F. and Samuels D. C., Science, **290** (2000) 777.
11. D. Kivotides, C. J. Vassilicos, D. C. Samuels and C. F. Barenghi, Europhys. Lett., **57**, 845 (2002)
12. D. R. Poole, H. Scoffield, C. F. Barenghi, and D. C. Samuels, J. Low Temp. Phys.,**132**, 97 (2003)
13. K.W. Schwarz, Phys. Rev. B **31**, 5782 (1985).
14. K.W. Schwarz, Phys. Rev. B **38**, 2398 (1988).
15. D.C. Samuels, Phys. Rev. B **46**, 11714 (1992).
16. R. G. K. M. Aarts and A. T. A. M. de Waele, Phys. Rev. B 50, 10069 (1994).
17. A. W. Baggaley and Laizet, Phys. Fluids **25**, 115101 (2013).
18. A. W. Baggaley, J. Laurie, J. Low Temp. Phys. **178**, 35(2015)
19. S. Yui and M.Tsubota,Phys. Rev. B **91**, 184504 (2015).
20. D. Khomenko, L. Kondaurova, V.S. L'vov, P. Mishra, A. Pomyalov and I.Procaccia, Phys. Rev. B **91**, 180504(R), 2015.
21. J. T. Tough, in Progress in Low Temperature Physics, edited by D. F. Brewer (North-Holland, Amsterdam, 1982), Vol. VIII, Chap. 3.
22. L. Galantucci, M. Sciacca, and C. F. Barenghi, Phys. Rev. B **92**, 174530 (2015)
23. A.W. Baggaley, C. Barenghi,Phys. Rev. B **83**,134509(2011)
24. L. Gamet, F. Ducros, F. Nicoud, and T. Poinsot, International Journal for Numerical Methods in Fluids **29**, 2 (1999).
25. L. Kondaurova, V.S. L'vov, A. Pomyalov and I. Procaccia, Phys. Rev. B **89**, 014502 (2014).
26. R. J. Donnelly and C. F. Barenghi, J. Phys. Chem. Ref. Data **27**, 6, (1998).
27. D. Khomenko, V. S. Lvov, A. Pomyalov, and I. Procaccia, Phys. Rev. B, **93**,134504(2016)